**ROYAL SOCIETY OF CHEMISTRY**

## PAPER

Check for updates

# Structural, morphological, and optical properties of SiC/PVP nanocomposite materials by changing the SiC concentration in PVP

Lala Gahramanli, [ID] *ab Maarif Jafarov,b Mustafa Muradov,a Telkhanim Mahmudova,a Shafiga Alakbarova,a Zeynab Addayeva,a Orkhan Gulahmadov, [ID] c Vusal Mammadov,b Rana Khankishiyeva, [ID] de Cristian Vacacela Gomez, [ID] fg Christos Trapalis,h Vitalii Yevdokymenko,i Kamenskyh Dmytro [ID] i and Talia Tenej

Silicon carbide (SiC) nanotubes with a one-dimensional structure were successfully synthesized *via* the carbothermal method at 1800 °C. SEM results revealed a hollow interior and rough surface morphology. These SiC nanotubes were incorporated into a polyvinylpyrrolidone (PVP) matrix to produce SiC/PVP composite materials with different filler concentrations (1–5 wt%). XRD analysis confirmed the presence of the cubic 3C–SiC phase. SiC nanotubes were incorporated into a PVP polymer matrix at concentrations of 1, 2, 3, and 5 wt% SiC. Scanning electron microscopy (SEM) images revealed the morphology of the nanotubes of pure SiC. Energy-dispersive X-ray spectroscopy (EDS) and elemental mapping showed a non-uniform SiC distribution across the polymer, with the most uniform dispersion occurring at 3 wt%. X-ray diffraction (XRD) results indicated a decrease in crystallite size as SiC content increased, with the smallest crystallite size (11.86 nm) occurring at 3 wt% SiC/PVP. The microstrain and dislocation density also exhibited a similar trend, increasing from 1 wt% (0.00587) to 3 wt% (0.00698) and then decreasing at 5 wt% SiC/PVP (0.00271). Ultraviolet-Visible (UV-Vis) spectroscopy revealed a band gap reduction from 5.62 eV at 1 wt% to 5.51 eV at 3 wt% SiC/PVP, with a slight increase to 5.70 eV at 5 wt% SiC/PVP, indicating the most favorable optical properties at 3 wt% SiC/PVP composite materials. Fourier-transform infrared (FTIR) spectroscopy confirmed the physical interaction between SiC and PVP, characteristic Si–C stretching bands at 700–1000 $cm^{-1}$, as well as the interaction of PVP carbonyl (C=O) and C–N groups with Si–O/–OH groups on the SiC surface without any covalent bonding formation. The 3 wt% SiC/PVP composite demonstrated optimal dispersion, crystallite refinement, and optical properties, indicating its potential as the optimal loading concentration for electronics and semiconductors, optical devices, and energy storage and conversion, making it an ideal material for advanced technological uses.

*aNano Research Laboratory, Center of Excellence, Baku State University, Baku, Azerbaijan. E-mail: lalagahramanli@bsu.edu.az; gahraman.lala@gmail.com*

*bFaculty of Physics, Chemical Physics of Nanomaterials, Baku State University, Baku, Azerbaijan*

*cFaculty of Engineering, Karabakh University, Khankendi, AZ2600, Azerbaijan*

*dInstitute of Radiation Problems, Ministry of Science and Education of the Republic of Azerbaijan, Baku, AZ1143, Azerbaijan*

*eDepartment of Physics and Chemistry, Azerbaijan University of Architecture and Construction, Baku, AZ1073, Azerbaijan*

*fUniversidad Ecotec, Km. 13.5 Samborondón, Samborondón, EC092302, Ecuador*

*gDepartment of Environmental Engineering (DIAm), University of Calabria, Via P. Bucci, Cubo 42B, 87036 Rende, Italy*

*hInstitute of Nanoscience and Nanotechnology, National Center for Scientific Research "Demokritos", Agia Paraskevi, 15341, Greece*

*iInstitute of Bioorganic Chemistry and Petrochemistry, N. A. S. of Ukraine, 50, Kharkivske Shose, Kiev, 02160, Ukraine*

*jDepartment of Chemistry, Universidad Técnica Particular de Loja, Loja 110160, Ecuador*

## 1 Introduction

In recent times, the preparation of polymer nanocomposites has enabled the creation of composites with different properties, depending on the shape and properties of the nanostructure used and the type of polymer, thereby expanding the application areas of nanocomposite materials. Among them, silicon carbide, which combines 50–50% to form nanostructures of various shapes due to covalent bonds, is a ceramic material that has attracted attention in the last 10 years with its optical, electrical, and thermal properties.[1] At the same time, their wide $E_g$ value range, mechanical strength, and chemical stability greatly increase the interest in the creation of nanocomposite materials based on them, which expands the possibility of using them in various fields of industry.[2,3] There are various polytypes of SiC, such as 3C–SiC (β-SiC), 4H–SiC, and 6H–SiC, which are distinguished from each other by their

different structures, $E_g$ values, and other properties.[4] Thus, 3C–SiC has $E_g$ values of 2.36 eV, 4H–SiC ~3.23 eV, and 6H–SiC ~3.0 eV.[5] This wide band gap minimizes electron–hole pair generation, reduces light absorption, and renders SiC suitable for optical devices such as LEDs, lasers, and photodetectors.[6] Its high thermal conductivity and chemical inertness also make SiC ideal for high-temperature, high-frequency, and harsh-environment applications.[7] Additionally, SiC supports point defects, such as Si vacancies and divacancies, that are optically addressable at room temperature and function as single-photon sources for quantum photonics.[8]

Polyvinylpyrrolidone (PVP), polystyrene (PS), poly(methyl methacrylate) (PMMA), polyethylene (PE), and polyvinyl alcohol (PVA) polymers are widely used in the preparation of nano-composite materials.[9–12] In particular, PVP is a promising matrix due to its stability, ease of processing, and good optical properties.[13] PVP is widely used as a steric stabilizer, capping agent, and adhesion promoter in hybrid inorganic–polymer systems because its pyrrolidone carbonyl can coordinate metal and semiconductor surfaces.[14] At the same time, its vinyl backbone provides solution processability.[15]

There are numerous research studies in the literature on the preparation of SiC in the form of composite materials with various types of polymers and the study of their properties.[16] Across silicon- and carbide-based nanostructures, it has been used to (i) control nucleation and growth, (ii) disperse ceramic nanoparticles in both aqueous and non-aqueous media, and (iii) tune optical/electrical responses of thin films and bulk nanocomposites.

Kadhim *et al.* (2020) prepared PVP films with 2–6 wt% SiC and observed that with higher SiC loading, the films' overall absorbance in the UV region rose, while transmittance fell. Crucially, the estimated energy band gap (indirect) decreased from about 3.7 eV (pure PVP) to 2.8 eV at 6% SiC.[13] This substantial band gap narrowing ($\approx 0.9$ eV) was attributed to improved charge transport and the creation of new energy levels within the band structure due to SiC.[13] Essentially, adding SiC introduced mid-gap states or extended the band tails, enabling optical transitions at lower photon energies.

In one research study on a PMMA/PC polymer blend, adding up to 0.8 wt% SiC decreased the intensity of the polymer's main amorphous peak. It broadened it, indicating increased amorphous character and disrupted polymer packing.[17] This suggests that SiC nanoparticles intercalate between polymer chains and reduce semi-crystalline domains. FTIR results of PMMA/PC–SiC composite, the major polymer bands (C=O stretch, C–H bends, *etc.*) remained at the same wavenumbers after SiC addition, but some peak intensities decreased.[13] This intensity reduction, without new peaks, indicates a predominantly physical interaction: SiC is well-dispersed among the polymer chains, causing some hydrogen-bonding or dipole interactions that can dampen certain vibrational modes, but no chemical reaction (no new functional groups) occurs.[13] The authors attributed this to weak physical forces between SiC and the polymer matrix rather than the formation of strong chemical bonds.[13] In another study, a PVA/PVP polymer blend was investigated at 0.5 wt%, 1 wt%, and 1.5 wt% filler

concentrations (SiC), and the absorbance of PVA/PVP is increased, while the transmittance is decreased with an increase in the SiC nanoparticles' concentration.[18] The energy gap of PVA/PVP is decreased when the SiC nanoparticles' concentration increases. The authors noted that higher SiC concentration yielded higher absorption in the UV range and a clear band gap reduction, underscoring the material's potential in optical applications.[18] Finally, the results on optical characteristics indicate that the PVA/PVP/SiC nanostructures can be considered as promising materials for optical fields. Similarly, other nanoparticle systems (PVP with ZnO, BaTiO$_3$, *etc.*) have also shown band gap decreases with fillers, high-lighting that nanoparticles act as dopants, creating sub-bandgap states or widening the absorption spectrum of polymer films.[18,19] Rashid *et al.* (2023) examined a PAA with SiC for solar thermal applications. Even in this case, they found that increasing SiC from 12.5 to 50 g L$^{-1}$ significantly depressed the optical band gap (for allowed transitions, from ~3.25 eV down to ~2.95 eV).[19] The indirect band gap similarly dropped from 3.15 to 2.90 eV with added SiC.[19] Alongside, the absorption at 400 nm rose by over 50% at the highest SiC content.[19] This shows that even in different polymer hosts, SiC nanoparticles consistently enable easier optical excitation (lower $E_g$), likely by providing extra electronic states and stronger light absorption.

Sarada and Muraleedharan (2016) reported on SiC-infused polystyrene and found the band gap energy of PS dropped with increasing SiC content, accompanying enhanced UV absorption of the nanocomposite films.[20] Though PS is a hydrophobic, non-polar polymer (unlike PVP, which is polar), the result was analogous: the $\pi \rightarrow \pi^*$ transitions in PS became easier (lower energy) when SiC was present, again pointing to the generality of band gap tuning by SiC across polymer types.[20]

For SiC–polymer systems, rheological studies establish how PVP improves dispersion. Xiao *et al.* fixed the total dispersant at 0.3 wt% (PAA + PVP) and showed that co-addition at pH $\approx 6$ yields Newtonian, low-viscosity aqueous SiC suspensions *via* electrosteric stabilization; the benefit diminishes in alkaline conditions where PAA is fully dissociated.[21] In non-aqueous media (EtOH/MEK), Zhang *et al.* identified PVP/SiC = 17 mg g$^{-1}$ as the optimal mass ratio for a stable, highly loaded suspension, with best wettability when EtOH comprised 40–50 wt% of the solvent blend.[22]

Beyond oxides, PVP also reshapes interfacial redox dynamics on Si.[23] In a metal-assisted chemical etch (MaCE) study, Chen & Hsiao *et al.* varied a PVP parameter, PVP over 5, 1, 0.1, 0.01, and 0 during Ag$^+$/HF etching; PVP drove Ag dendrites to favor (111) facets over (200), switching Si dissolution from wire-forming to nearly isotropic surface polishing. While not a polymer composite, this work underscores PVP's strong, selective adsorption on metal surfaces – relevant for charge-transfer and adhesion at SiC–polymer interfaces.

Thin-film optics research highlights PVP's adhesive role. Thompson & Zou used a 1 wt% PVP adhesion layer beneath 5 wt% SiO$_2$ nanoparticle antireflective coatings, lifting average glass transmittance from ~95% to >98% and boosting Si cell short-circuit current.[24] The result supports a generalizable view:

PVP often acts as a molecular bridge that improves inorganic particle integration and optical uniformity.

Most existing works on PVP-based nanocomposites use polymer blends where the individual role of PVP is convoluted, and systematic characterization, like structural, optical, and morphological properties, is missing in the literature. As evidenced by previous SiC/polymer studies, Kadhim *et al.* reported band-gap narrowing in PVP/SiC films but mainly analysed optical constants from UV-Vis spectra without a detailed structural or vibrational investigation of the PVP–SiC interface.[13] In PMMA/PC–SiC and PVA/PVP–SiC blends, Alhusaiki-Alghamdi and *et al.* showed that SiC addition modifies amorphous structure and decreases the optical band gap, yet the individual contribution of each polymer and the specific interfacial chemistry around SiC remain convoluted by the presence of two host polymers.[17,18] Rashid *et al.* demonstrated similar band-gap reduction and enhanced absorption in PAA/SiC systems designed for solar thermal applications, while Sarada *et al.* revealed SiC-induced band-gap changes and altered thermal degradation in PS-based nanocomposites.[19,20] More recently, Gahramanli *et al.* carried out a comprehensive multi-technique study on PVA/SiC nanocomposites over a broad 1–10 wt% range and correlated SiC loading with structural, optical, and dielectric properties; however, the focus was on an OH-rich PVA matrix and on identifying an optimum composition for dielectric performance rather than on the low-loading, interface-dominated regime in a pure PVP host.[25] Consequently, none of these works provides a systematic, quantitative correlation between interfacial spectroscopic signatures (FTIR/Raman), dispersion and microstructure (XRD/SEM), and band-gap modulation in transparent PVP/SiC nanocomposite films at low SiC contents. To understand the interaction between nanostructure and polymer, the dependence of filler concentration needs to be investigated for tailoring such materials for advanced functional applications.

Additionally, we note that most previous PVP/SiC studies have employed approximately spherical or irregular SiC nanoparticles as the filler phase,[13,18] whereas in the present work, we use SiC structures with a nanotube-like morphology. This anisotropic, one-dimensional geometry increases the interfacial contact area and can modify percolation, scattering, and band-gap behaviour compared with equiaxed nanoparticles, particularly at low loadings. Furthermore, our study combines XRD (including crystallite size evaluation at 1–5 wt% SiC), FTIR analysis of the PVP carbonyl and ring vibrations, and SEM–EDS elemental mapping to assess both the structural evolution and the spatial distribution of SiC within the PVP matrix. In contrast to Kadhim *et al.*, who examined three SiC concentrations and focused mainly on optical and electrical parameters,[13] we investigate finely stepped loadings from 1 to 5 wt% and specifically follow how small changes in SiC content affect the optical band gap ($E_g$) and interfacial vibrational signatures. This low-loading, high-resolution concentration mapping is important for identifying possible transition or "optimal" compositions and for formulating interfacial structure–property relationships in SiC/PVP nanocomposites.

In the presented study, the properties of SiC/PVP composites are investigated depending on filler concentration in the PVP polymer matrix, and the influence of filler concentration on structural, optical, and morphological properties is systematically investigated. This study systematically investigates PVP/SiC nanocomposites at low SiC loadings (1–5 wt%). In this study, we focus on SiC/PVP nanocomposites at low SiC loadings (1–5 wt%) in an interface-dominated and still optically transparent regime. Building on the optical study of SiC/PVP films by Kadhim *et al.*,[13] we aim to go beyond band-gap estimation and to correlate interfacial chemistry and dispersion state with optical response by combining XRD, FTIR, Raman, UV-vis, and SEM/EDS. To the best of our knowledge, such a multi-technique, quantitative correlation for nanotube-like SiC fillers in a pure PVP host at low SiC contents has not yet been reported.

## 2 Experimental part

### 2.1. Materials and methods

PVP was used as the polymer matrix. High-purity $SiO_2$ and activated carbon (Farmak, Ukraine) were mixed to form a uniform blend and placed in a graphite crucible. The mixture was air-dried and subjected to carbothermal reduction in a VCI-3.5 furnace under vacuum and argon atmosphere to synthesize SiC. The reaction setup is shown in Fig. 1, based on the high-temperature reaction of $SiO_2$ with carbon to produce SiC and CO.[25]

The formation of SiC occurs through the reduction of $SiO_2$ by carbon at elevated temperatures in the precursor ratio ($SiO_2 : C$) 1 : 1, following the reactions summarized below:

$$SiO_2 + C \rightarrow SiO + CO \qquad (1)$$

$$SiO + C \rightarrow SiC + CO$$
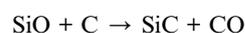
Before heating, the furnace chamber was evacuated to approximately 950 mbar, then purged and filled with argon gas at a constant flow rate maintained between 6 and 12 L h$^{-1}$
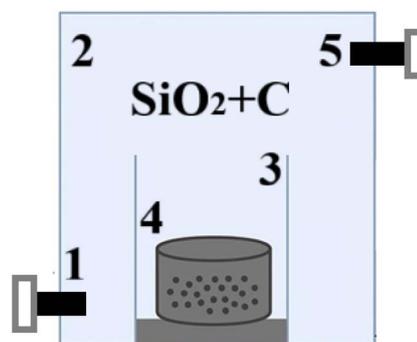


Fig. 1 Reaction furnace for obtaining SiC nanostructures: 1-gas in; 2-heating furnace; 3-heating unit; 4-graphite crucible; 5-pump switch.

throughout the process. The carbothermal reduction was conducted at a temperature of 1800 °C for 1 h using a single-step heating program with a ramp rate of 10 °C min$^{-1}$. Upon completion of the reaction, the system was cooled to room temperature under an inert atmosphere at a controlled rate of 20 °C min$^{-1}$. To eliminate traces of unreacted carbon, the as-synthesized SiC powders were subjected to a post-treatment in a muffle furnace at 800 °C for 30-minute intervals in the presence of air. The final SiC products exhibited a color transition from grey to light green, which was found to vary with the synthesis temperature.

To prepare composite materials, in the first stage of the experiment for the preparation of SiC/PVP nanocomposites, 0.5 g of PVP powder was taken, and 20 mL of a mixture of ethanol and DW was used. The mixture was placed in a glass flask and carried out reflux system. The solution was continuously stirred with a magnetic stirrer at 70–80 °C for about 2 hours. This step ensured the complete dissolution of PVP into the solvent and the formation of a homogeneous solution. Separately, a certain amount of appropriate filler concentration (1 wt%, 2 wt%, 3 wt%, 5 wt%) of previously prepared SiC nanostructures was dispersed in 10 mL of ethanol and DW mixture. This suspension was first manually stirred for 5 minutes, followed by ultrasonication for 15 minutes to achieve better dispersion. At the final stage, the nanocomposite solution was cast into Petri dishes and left to dry at room temperature, forming thin SiC/PVP nanocomposite materials. After drying, the films were subjected to hot pressing using molds of 3 cm diameter, under a pressure of 10 MPa at 150 °C for 30 seconds (close to the softening temperature of PVP), and then cooled rapidly. Cooling rate was $\approx 20$ (°C min$^{-1}$), and $\Delta T$ was from 150° to 25 °C. The concentration of the SiC/PVP composites was calculated according to eqn (2):

$$\text{Concentration (\%)} = \text{SiC/PVP} \times 100\% \qquad (2)$$

The general procedure for obtaining SiC/PVP nanocomposites is shown schematically in Fig. 2.

### 2.2. Characterization technique

The XRD analysis was performed using a Bruker D8 Phaser in the range of 5–80° 2$\theta$ with a step size of 0.02° 2$\theta$. The morphology, EDS analysis, and element mapping of the nanocomposites were examined by SEM using an FEI Quanta Inspect microscope (FEI, Hillsboro, OR, U.S.A.) equipped with a tungsten filament. Chemical bonds were identified using FTIR spectra collected in the 400–4000 cm$^{-1}$ wavenumber range using an IR Affinity FTIR spectrometer (Shimadzu, Japan). To determine the transmittance spectrum and band gap values, UV-Vis spectrophotometer (Model Specord 250 PLUS, Analytik Jena AG, Germany) was used.

## 3 Results and discussions

### 3.1. Morphological analysis

SEM was used to investigate the morphology of synthesized SiC nanostructures and the dispersion of SiC nanotubes within the PVP matrix. The SEM images of the pure SiC nanostructures are shown in Fig. 3.

SEM images showed that 1D nanotubes can be obtained by the carbothermal method at 1800 °C. When looking at the morphology of nanotubes, it is clearly seen that they have different sizes of hollow inside and rough surfaces. Fig. 4 shows SEM images, EDS, and element mapping of composite materials of SiC nanotubes with different percentages in PVP polymer.

SEM images of the composite materials show that in the 1 wt% SiC/PVP (Fig. 4a) sample, SiC nanotubes are mainly located within the pores of the PVP matrix, and the surface is smoother than in other samples. In the 2 wt% SiC/PVP (Fig. 4c) composite, it is possible to see that nanostructures fill the pores and form islands on the surface of the polymer. In the 3 wt% SiC/PVP (Fig. 4e) sample, it is evident that SiC nanostructures aggregate on the polymer surface, forming larger islands. In the 5 wt% SiC/PVP (Fig. 4g) sample, large aggregates are formed on the polymer surface, and the roughness of the surface is clearly visible.

For all composite materials, the elemental distribution across the surface was analyzed using EDS and elemental mapping. In Fig. 4b, for the 1 wt% SiC/PVP composite, the atomic fraction of C is 26% (wt% = 31.90%), Si is 1.43% (wt% = 0.24%), and O is 72.57% (wt% = 66.84%). The high fraction of C in all samples is associated with the polymeric substrate used. At the same time, the low amount of Si indicates a small content of SiC within the polymer matrix. Moreover, elemental mapping confirms a non-uniform distribution. For the 2 wt% SiC/PVP
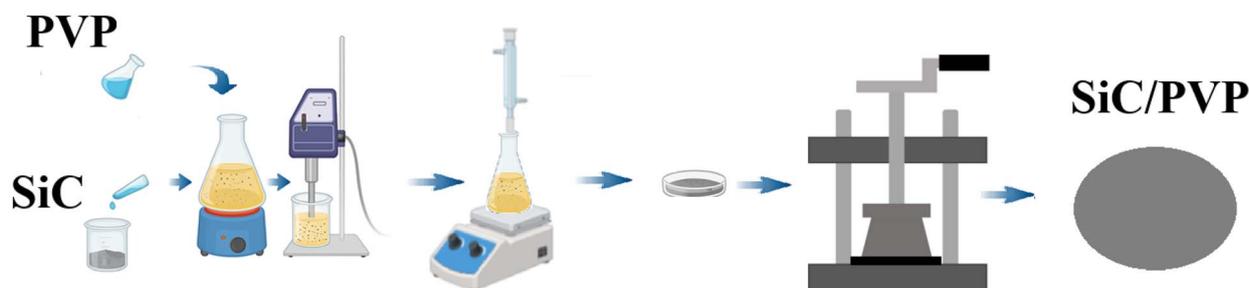


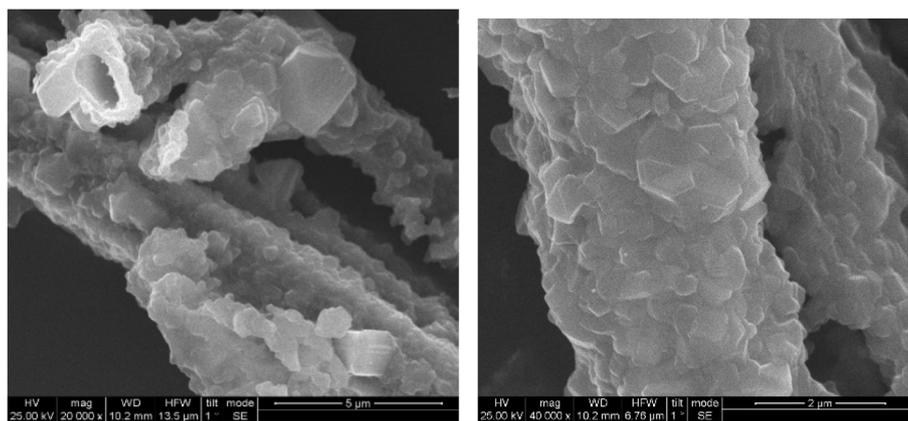**Fig. 2** Schematic illustration of the synthesis of SiC/PVP nanocomposite materials.

**Fig. 3** SEM images of pure SiC nanostructures.

composite, the atomic fractions are 21.85% C (wt% = 28.19%), 9.33% Si (wt% = 5.15%), and 68.83% O (wt% = 66.67%). Compared to the 1 wt% SiC/PVP sample, the Si content is higher, which is evident both from the atomic fraction and from the bright regions corresponding to Si in the elemental map. Elemental mapping shows that SiC is relatively more densely distributed within the polymer and on the surface. For the 3 wt% SiC/PVP composite, the atomic fractions are 16% C (wt% = 1.97%), 19.35% Si (wt% = 11.36%), and 64.66% O (wt% = 66.67%). Here, the Si content is higher than in all other composites, and the mapping clearly shows that SiC is more densely and uniformly distributed within the polymer matrix. For 5 wt% SiC/PVP, the atomic fractions are 25.74% C (wt% = 31.54%), 1.54% Si (wt% = 1.54%), and 72.72% O (wt% = 66.91%). Elemental mapping reveals that Si appears as bright, clustered regions rather than being dispersed within the polymer. This indicates a non-homogeneous microstructure in which SiC particles tend to aggregate into dense clusters instead of being uniformly distributed.

### 3.2. Structural analysis

XRD was used to identify the crystalline phases, evaluate structural regularity, and estimate the crystallite size of pure SiC and the PS polymer matrix, as well as different concentrated composite materials, as shown in Fig. 5.

From the XRD pattern, the peak observed at 2-theta = 35.35° corresponds to the (111) Miller indices.[26] The other peak at 2-theta = 41.10° corresponds to the (200) index.[27] The peak observed at 2-theta = 59.72° corresponds to the (220) index.[28] For 2-theta = 71.49° corresponds to the (311) Miller index.[29] The observed peaks are attributed to the cubic phase of SiC and are known as 3C–SiC phases. The size of the crystallite for pure SiC is determined to be 9.11 nm.

Two broad amorphous halo peaks were observed near 2-theta = 11.40° and 20.84° in the XRD pattern of the pure PVP polymer, which is consistent with recent reports by Zidan *et al.*, describing similar halo features in the diffraction pattern of amorphous PVP.[30]

In the XRD patterns of the composite materials, peaks belonging to both PVP and SiC are observed. Thus, in the 1 wt%

SiC/PVP composite, the characteristic peak belonging to SiC is explained by the small percentage of SiC within PVP and its even distribution within the PVP chains. In the 2 wt% SiC/PVP composite material, the characteristic diffraction patterns belonging to SiC are clearly observed. With an increase in the concentration to 3 wt%, the intensity of the diffraction peaks increased. This is due to the fairly homogeneous dispersion of SiC nanostructures in the PVP matrix. In the 5 wt% SiC/PVP composite, although the diffraction peaks belonging to SiC are observed, their intensity has significantly decreased, and at the same time, halo peaks belonging to PVP are also observed. This phenomenon is explained by several factors. First, the increase in the concentration of SiC structures within the PVP matrix leads to an increase in their mutual attraction forces within the matrix and, as a result, the agglomeration process. The aggregation of particles results in a decrease in the effective surface area for diffraction, reducing the overall intensity of the SiC peaks.[31] Second, the abundance of SiC nanostructures restricts the movement of PVP chains, as a result of which the local disorder of the polymer increases and the share of the amorphous component increases.[32] This is manifested in the re-intensification of the amorphous halo peak in the diffraction pattern. Thus, the addition of SiC in the range of 1–3 wt% leads to the formation of crystalline areas in the PVP matrix and an increase in the intensity of the diffraction peaks. However, at 5 wt% SiC/PVP, due to the rise in SiC and the tendency of the particles to agglomerate, as well as the strengthening of the amorphous nature of the polymer matrix, the intensity of the SiC peaks decreases, and the halo peaks again become dominant.

Table 1 shows the crystallite sizes, microstrain values, and dislocation densities of the composite materials calculated using Debye–Scherrer.

As can be seen from Table 1, for the 1 wt% SiC/PVP sample, the crystallite size is 20.20 nm, and the microstrain is 0.00587, whereas for the 3 wt% SiC/PVP sample, the crystallite size decreases to 11.86 nm and the microstrain increases to 0.00698. This behavior can be attributed to the improved dispersion of SiC nanostructures and the resulting increase in internal lattice stress. The SiC phase restricts the crystallization of the PVP matrix, causing local deformation. While the dislocation
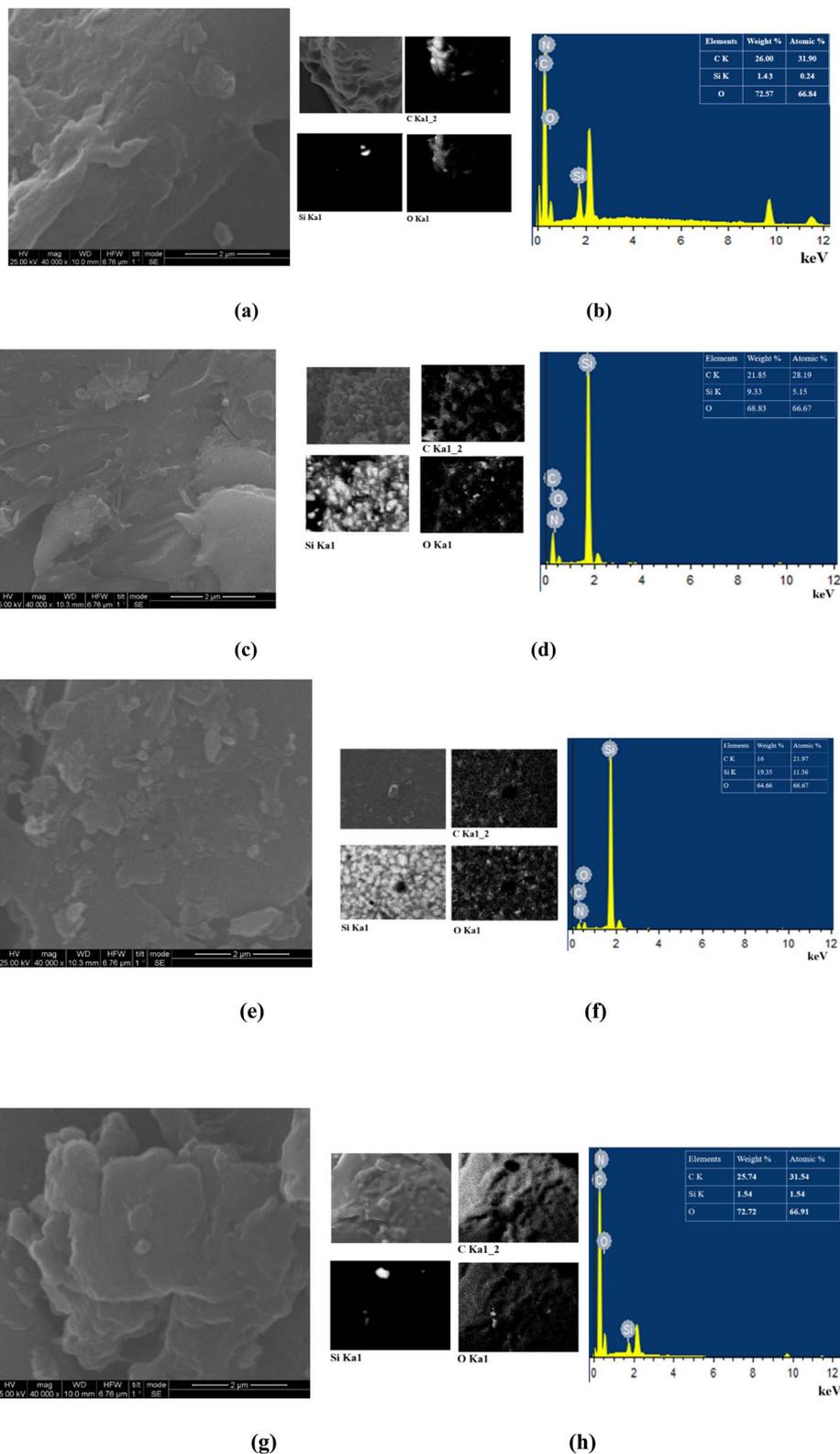
Fig. 4   SEM images, EDS analysis, and element mapping of SiC/PVP composite materials SEM images: (a) 1 wt% SiC/PVP; (c) 2 wt% SiC/PVP; (g) 3 wt% SiC/PVP; (e) 5 wt% SiC/PVP EDS and element mapping: (b) 1 wt% SiC/PVP; (d) 2 wt% SiC/PVP; (f) 3 wt% SiC/PVP; (h) 5 wt% SiC/PVP.

density ($\delta$) is $3.27 \times 10^{15}$ m$^{-2}$ for 1 wt% SiC/PVP, it reaches $6.62 \times 10^{15}$ m$^{-2}$ for the 3 wt% sample, which is associated with the higher concentration of defects and the proliferation of grain boundaries. Because smaller crystallites generate a larger total grain-boundary area, the dislocation density increases as the crystallite size decreases.
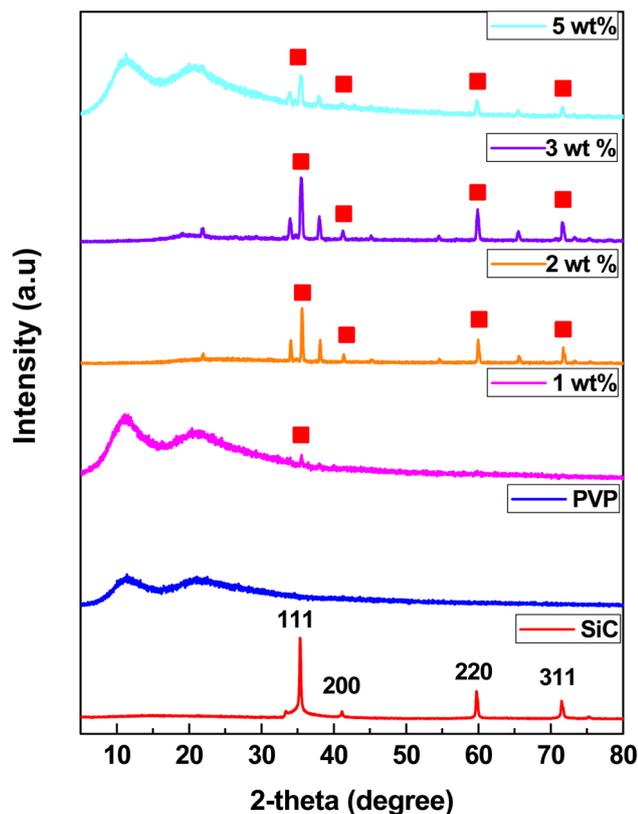
**Fig. 5** XRD pattern of pure SiC, PVP, and SiC/PVP-based composite materials.

**Table 1** Crystallite sizes, microstrain values, and dislocation densities of SiC/PVP composite materials

| Samples | Crystallite size, nm | Microstrain | Dislocation density |
|---------|---------------------|-------------|---------------------|
| 1 wt% SiC/PVP | 20.20 | 0.00587 | $3.27 \times 10^{15}$ |
| 2 wt% SiC/PVP | 13.43 | 0.00749 | $6.27 \times 10^{15}$ |
| 3 wt% SiC/PVP | 11.86 | 0.00698 | $6.62 \times 10^{15}$ |
| 5 wt% SiC/PVP | 16.17 | 0.00271 | $1.88 \times 10^{15}$ |

A direct positive correlation is observed between microstrain and dislocation density: as the microstrain increases, the dislocation density also increases. This trend is related to the increase in internal lattice stress and the consequent multiplication of defects and dislocations. The relatively high microstrain and dislocation density values in the 2 wt% and 3 wt% SiC/PVP samples support this relationship. With increasing SiC content, the crystallite size initially decreases, whereas both microstrain and dislocation density increase. However, at higher filler loading (5 wt%), partial growth of crystallites occurs due to aggregation of the SiC nanostructures, leading to a reduction in both microstrain and dislocation density. These results suggest that SiC nanostructures establish an equilibrium between optimal dispersion and crystal-lattice stress in the PVP matrix. Therefore, the SiC content of 2–3 wt% SiC/PVP can be considered an optimal range, with 3 wt% providing the most pronounced refinement of crystallites and the highest defect density before aggregation effects appear at 5 wt% SiC/PVP.

### 3.3. Ultraviolet-Visible spectroscopy

UV-Vis spectroscopy was applied to investigate the optical absorption characteristics of the SiC/PVP nanocomposites, and direct band gap values can be determined by the Tauc relation $(\alpha h\nu)^2$–$(h\nu)$ dependence.[33] In Fig. 6, the absorbance spectrum of pure SiC (Fig. 6a) and composite materials (Fig. 6b) is shown.

According to the absorbance spectrum, Tauc plots were used to determine band gap values for pure SiC and PVP, as well as different concentrated SiC/PVP nanocomposite materials.[18] Tauc plots for pure SiC (Fig. 7a), pure PVP (Fig. 7b), and for 1–5 wt% SiC/PVP nanocomposite materials (Fig. 7c–f) are illustrated in Fig. 7.
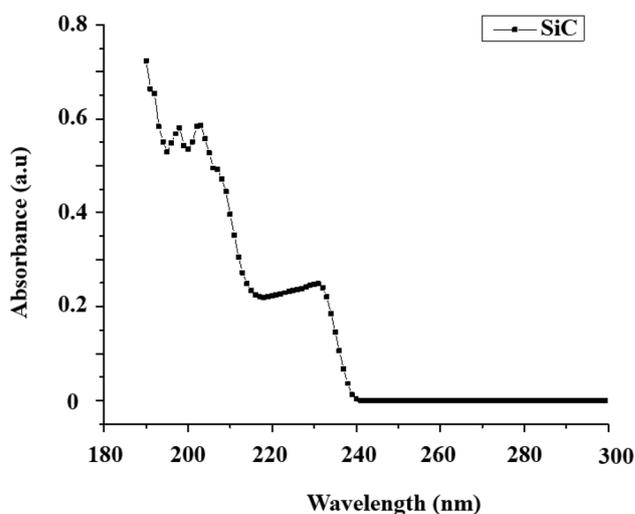


(a)
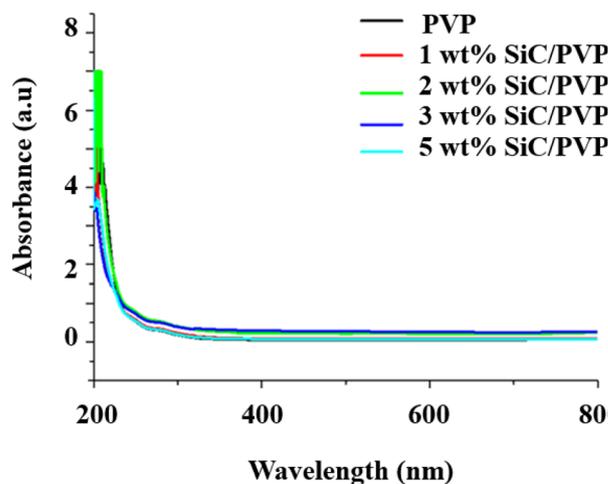


(b)

**Fig. 6** Absorbance spectrum of (a) pure SiC and (b) SiC/PVP composite materials.

As shown in Table 2, the $E_g$ values of pure SiC and PVP are approximately equal, at 5.76 and 5.78 eV, respectively. In the literature, the band gap of pure SiC has been reported as 3.2 eV,[34] while high-energy absorption edges near 5.9 eV have also been observed,[35] attributed to quantum-confinement effects in very small structures. These effects, combined with reduced defect-related absorption in well-prepared samples, can shift the apparent absorption edge to higher energies than the bulk band gap. Consequently, optical measurements on SiC nanocrystals may show absorption onsets in the 5–6 eV range, consistent with the values observed in the presented study. This value aligns with the reported direct $E_g \approx 6$ eV for 3C–SiC.[36] The use of nanostructured SiC (9–20 nm) and the direct-transition Tauc model naturally emphasizes this high-energy transition and may introduce a slight additional blue shift.[36] In the literature, the band gap value of PVP is close to the obtained value of 5.78 eV,[37] supporting our obtained results.
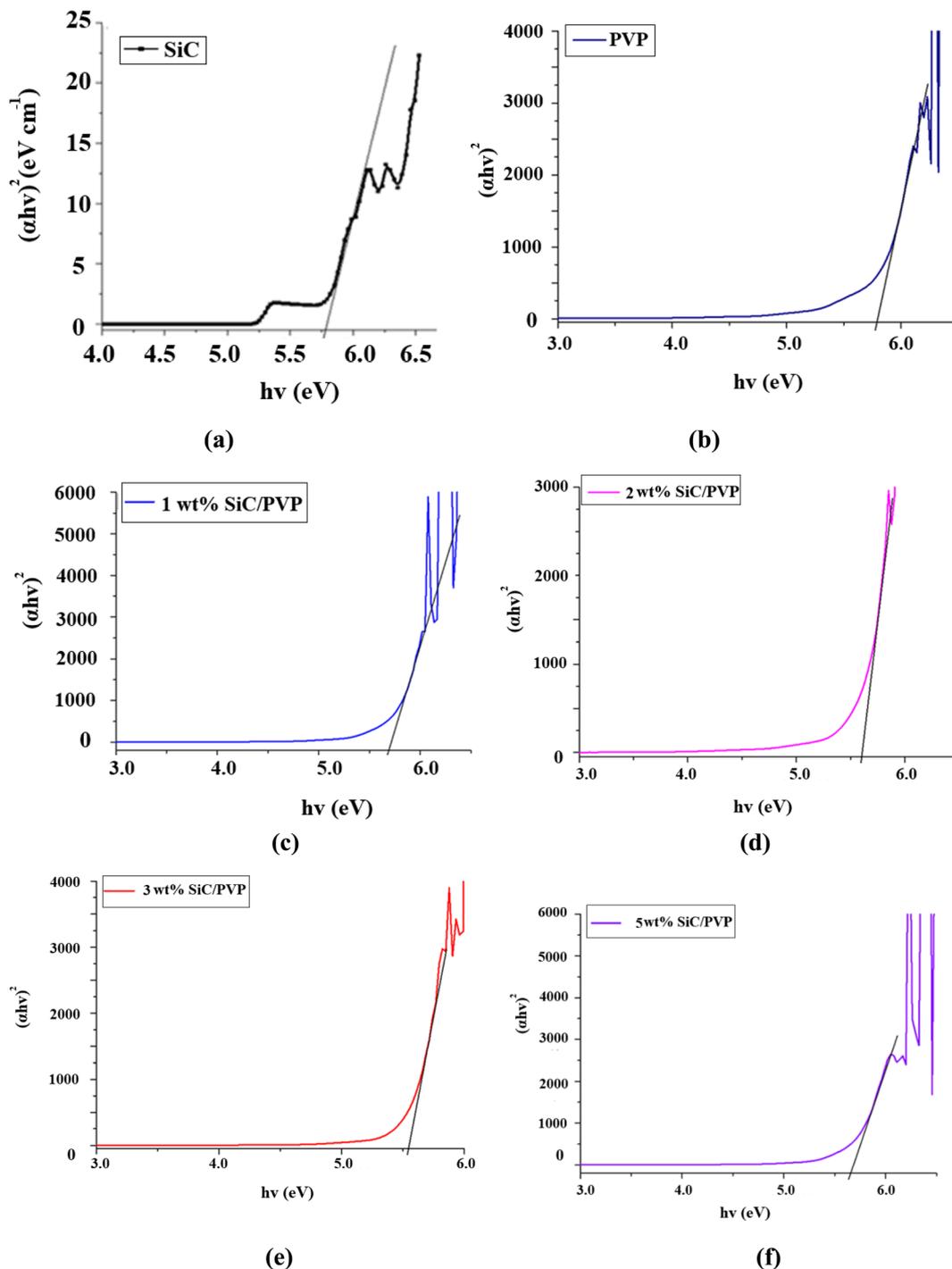


Fig. 7 Band gap determination of (a) SiC; (b) PVP; (c) 1% SiC/PVP; (d) 2% SiC/PVP; (e) 3% SiC/PVP; (f) 5% SiC/PVP.

**Table 2**  Band gap values by Tauc plots

| Samples | $E_g$, eV |
| --- | --- |
| SiC | 5.76 |
| PVP | 5.78 |
| 1 wt% SiC/PVP | 5.62 |
| 2 wt% SiC/PVP | 5.52 |
| 3 wt% SiC/PVP | 5.51 |
| 5 wt% SiC/PVP | 5.70 |

The $E_g$ value of 1 wt% SiC/PVP composite material is 5.62 eV, 2 wt% SiC/PVP is 5.52 eV, 3 wt% SiC/PVP is 5.51 eV, and 5 wt% SiC/PVP is 5.70 eV. When SiC nanostructures are incorporated into the PVP matrix, the $E_g$ decreases sequentially from 5.62–5.51 eV in the loading range of 1–3 wt%, which is mainly explained by the redshift of the absorption edge due to defects and localized energy states formed at the SiC–PVP interface. When the nanostructures are well dispersed, the interface area per unit volume increases, and a smaller $E_g$ is obtained in the Tauc extrapolation. However, when the loading reaches 5 wt%, the increase in $E_g$ to 5.70 eV is consistent with the reduction of the effective interface area due to aggregation at high loading. As a result, scattering effects prevail, and $E_g$ increases again. Considering both the microstructural parameters and the evolution of the optical band gap, the SiC content of 2–3 wt% SiC/PVP can be regarded as an optimal loading range. In particular, 3 wt% SiC/PVP exhibits the lowest $E_g$ (5.51 eV) together with well-dispersed nanostructures, whereas further increase to 5 wt% leads to aggregation, a reduction of the effective interface area, and a subsequent widening of the band gap.

### 3.4.  FTIR analysis

FTIR spectroscopy was conducted to analyze the molecular structure of the pristine PVP matrix, detect vibrational modes of SiC in PVP, and identify any changes in chemical bonding and interfacial interactions induced by filler incorporation. The FTIR spectrum of SiC (Fig. 8a) and different concentrated SiC/PVP composite materials (Fig. 8b) is shown in Fig. 8.

As can be seen from the FTIR spectrum of pure SiC (Fig. 8a), a strong absorption was observed in the 700–1000 cm$^{-1}$ range. This absorption is attributed to the $\nu$(Si–C) bond. In the scientific literature, the intense absorption band in the IR region from 700 cm$^{-1}$ to about 1000 cm$^{-1}$ for SiC in the cubic phase has been associated with the Si–C characteristic stretching mode.[38] In Fig. 8b, the deep absorption observed at 3400 cm$^{-1}$ for the pure PVP matrix is due to the –OH groups and the weak –OH hydrogen bond in PVP.[29,39] The 2950 cm$^{-1}$ –CH$_2$ asymmetric and symmetric stretching is due to the PVP skeleton. This type of "C–H stretch" band is typical in polymeric materials.[40] The C=O stretch of PVP at 1650 cm$^{-1}$ is characteristic of the carbonyl group of PVP. In the literature, C=O is given as ~1670 cm$^{-1}$ in the PVP-PVA spectra.[40] The band observed at 1490 cm$^{-1}$ in the spectrum is due to –CH$_2$ bending and ring vibrations (PVP).[41] The band at about ~1280 cm$^{-1}$ is a characteristic absorption of the C–N stretch of PVP.[42] The band in the range of ~1060–1010 cm$^{-1}$ may be related to Si–O–Si on the SiC surface—it is possible that a band in this region will appear as SiC increases.[39]

A slight shift and broadening of the lactam C=O ($\approx$1650–1660 cm$^{-1}$) band of PVP and small changes in the C–N region during the formation of composites with different percentages
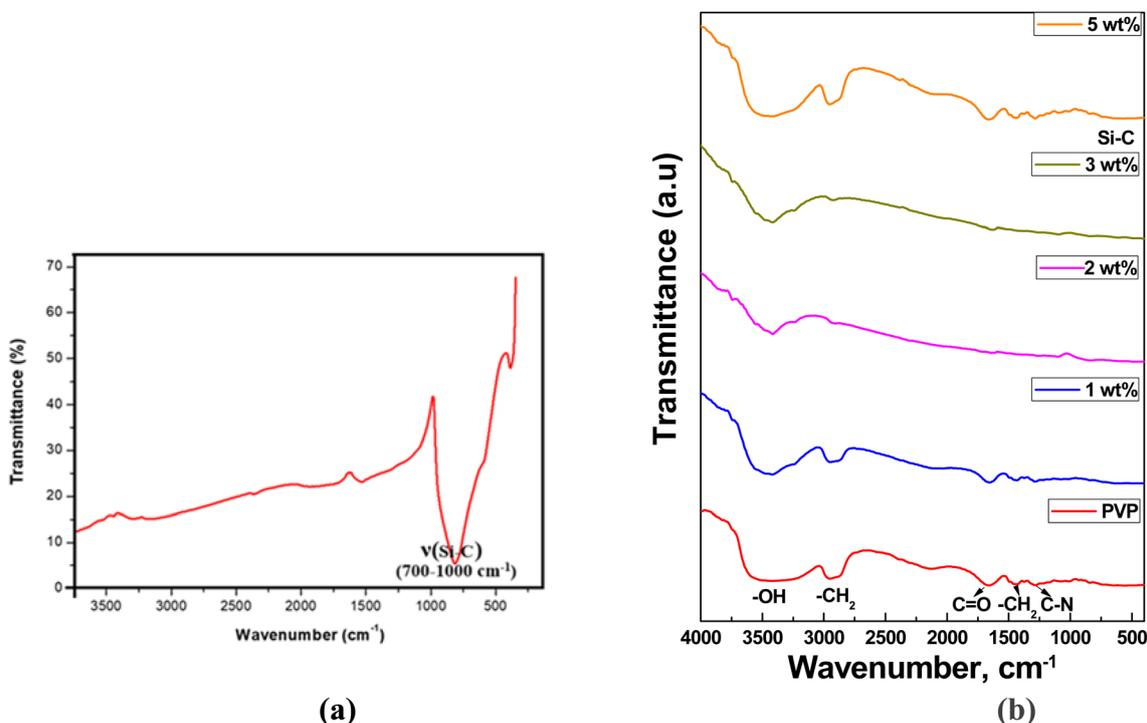




**Fig. 8**  FTIR spectrum of pure SiC (a) and different concentrated SiC/PVP nanocomposite materials (b).

indicate that the polymer carbonyl establishes hydrogen bonds and dipole interactions with the –OH/Si–O groups on the SiC surface. This is due to physical interactions rather than chemical reactions.[43] The band in the range of ~830–780 cm$^{-1}$ is due to the Si–C stretching characteristic of β-SiC. A band at ~813.96 cm$^{-1}$ has been reported for synthesized SiC nanostructures in the literature.[39,44] Thus, this band is enhanced with increasing SiC content in PVP.

The increasing intensity of the Si–C band around ~800 cm$^{-1}$, together with the low-frequency bands at 500–650 cm$^{-1}$, with increasing SiC content, indicates the higher fraction of SiC structures in the composite. The bands at ~650–600 cm$^{-1}$ and ~520–500 cm$^{-1}$, related to Si–C/Si–O low-frequency modes, appear or become more pronounced at high SiC loadings. As the SiC content increases from 1 to 5 wt%, the intensity of the Si–C band at ~800 cm$^{-1}$ systematically grows, while its position remains nearly unchanged (800 $\pm$ 3 cm$^{-1}$). The corresponding increase in the intensity ratio of the Si–C band to the PVP, C=O band confirms the progressive enrichment of SiC in the matrix and its good dispersion, without the formation of new covalent Si–C bonds between PVP and the filler. In contrast, the PVP bands at 3400, 2950, 1650 and 1280 cm$^{-1}$ gradually decrease in relative intensity with increasing SiC content, reflecting the reduced volume fraction (dilution) of the polymer phase and the partial immobilization of PVP chains in the interfacial region, which limits the effective transition dipole moment of these vibrations; additional attenuation may also arise from enhanced scattering at high filler loadings.[45,46] Importantly, the positions of the main PVP bands remain almost unchanged, indicating that the intrinsic vibrational frequencies of the polymer functional groups are essentially preserved and that the dominant effect of SiC addition is dilution and chain immobilization due to physical interactions, rather than weakening of the chemical bonds. Taken together, the evolution of the Si–C region and low-frequency modes, along with the concomitant attenuation of PVP bands, clearly demonstrates a consistent trend with SiC content and supports the conclusion that SiC nanostructures are successfully dispersed in the PVP matrix through hydrogen bonding and dipolar interactions rather than chemical reactions.

## 4 Conclusion

In this study, SiC nanotubes synthesized by the carbothermal method were successfully embedded into a PVP matrix to form SiC/PVP nanocomposites with variable filler content. XRD, SEM, EDS, and FTIR analyses confirmed the coexistence of cubic SiC nanostructures and amorphous PVP phases in composite materials. Elemental mapping confirmed that SiC was well-dispersed at moderate concentrations, particularly at 3 wt%, where the nanotubes were uniformly distributed, with minimal aggregation. XRD analysis revealed that the crystallite size decreased from 20.20 nm at 1 wt% to 11.86 nm at 3 wt%, with an associated increase in microstrain from 0.00587 to 0.00698. Dislocation density followed a similar trend, rising from 3.27 × 10$^{15}$ m$^{-2}$ at 1 wt% to 6.62 × 10$^{15}$ m$^{-2}$ at 3 wt%, before

decreasing at 5 wt% (1.88 × 10$^{15}$ m$^{-2}$). UV-Vis results showed a redshift in the band gap, with a minimum value of 5.51 eV for the 3 wt% SiC/PVP composite. FTIR spectroscopy indicated that SiC/PVP interactions were primarily physical, involving hydrogen bonding and dipole interactions rather than chemical bonding. These quantitative findings highlight 3 wt% SiC/PVP as the optimal concentration for achieving the best overall structural stability, crystallite refinement, and optical properties, making it the ideal choice for SiC/PVP composite materials in various applications.

## Author contributions

Lala Gahramanli: writing – review & editing, writing – original draft, visualization, validation, methodology, investigation, formal analysis, conceptualization. Mustafa Muradov and Maarif Jafarov: writing – review & editing, supervision, project administration. Telkhanim Mahmudova, Vitalii Yevdokymenko, and Kamenskyh Dmytro: methodology. Shafiga Alakbarova, Zeynab Addayeva, Orkhan Gulahmadov, and Christos Trapalis: formal analysis, Rana Khankishiyeva: formal analysis and investigation, Vusal Mammadov: investigation, Cristian Vacacela Gomez and Talia Tene: writing – review & editing.

## Conflicts of interest

The authors declare that they have no known competing financial interests or personal relationships that could have appeared to influence the work reported in this paper.

## Data availability

The data that support the findings of this study are available from the corresponding author upon reasonable request.

## References

1 O. Agboola, O. S. Fayomi, A. Ayodeji, A. O. Ayeni, E. E. Alagbe, S. E. Sanni, E. E. Okoro, L. Moropeng, R. Sadiku, K. W. Kupolati and B. A. Oni, *Membranes*, 2021, **11**, 139, DOI: 10.3390/membranes11020139.

2 Q. Shangguan, Y. Lv and C. Jiang, *Nanomaterials*, 2024, **14**, 1679, DOI: 10.3390/nano14201679.

3 X. Yin, S. Li, G. Ma, Z. Jia and X. Liu, *RSC Adv.*, 2021, **11**, 27338–27345, DOI: 10.1039/D1RA04604G.

4 H. Li, Z. Zhou, X. Cao, Z. Du, W. Yan, J. Li, A. Mujear, Y. Shao, J. Chen, X. Wang and G. Gao, *Prog. Nat. Sci.:Mater. Int.*, 2024, **34**, 12–25, DOI: 10.1016/j.pnsc.2024.01.014.

5 L. Zhou, T. Yang, E. Wang, X. Hou, Z. Fang and Y. Hou, *Adv. Funct. Mater.*, 2025, 2426020, DOI: 10.1002/adfm.202426020.

6 Y. Zou, Y. Zhang, Y. Hu and H. Gu, *Sensors*, 2018, **18**, 2072, DOI: 10.3390/s18072072.

7 Z. Cheng, J. Liang, K. Kawamura, H. Zhou, H. Asamura, H. Uratani, J. Tiwari, S. Graham, Y. Ohno, Y. Nagai and T. Feng, *Nat. Commun.*, 2022, **13**, 7201, DOI: 10.1038/s41467-022-34943-w.

8 G. Wolfowicz, C. P. Anderson, A. L. Yeats, S. J. Whiteley, J. Niklas, O. G. Poluektov, F. J. Heremans and D. D. Awschalom, *Nat. Commun.*, 2017, **8**, 1876, DOI: 10.1038/s41467-017-01993-4.

9 M. Namasivayam, M. R. Andersson and J. G. Shapter, *Polymers*, 2021, **13**, 2447, DOI: 10.3390/polym13152447.

10 L. Elbakyan and I. Zaporotskova, *Polymers*, 2024, **16**, 1242, DOI: 10.3390/polym16091242.

11 S. U. Rehman, S. Javaid, M. Shahid, I. H. Gul, B. Rashid, C. R. Szczepanski, M. Naveed and S. J. Curley, *Polymers*, 2022, **14**, 3576, DOI: 10.3390/polym14173576.

12 W. U. Khan, M. K. Bahar, H. Mazhar, F. Shehzad and M. A. Al-Harthi, *Adv. Compos. Hybrid Mater.*, 2023, **6**, 222, DOI: 10.1007/s42114-023-00802-5.

13 W. K. Kadhim, A. Hashim and M. A. Habeeb, Synthesis and Studying the Optical Parameters of Polyvinylpyrrolidone/SiC Nanoparticles, *J. Eng. Res. Technol.*, 2020, **9**(12), DOI: 10.17577/IJERTV9IS120154.

14 K. M. Koczkur, S. Mourdikoudis, L. Polavarapu and S. E. Skrabalak, *Dalton Trans.*, 2015, **44**, 17883–17905, DOI: 10.1039/C5DT02964C.

15 E. Browne, Z. A. Worku and A. M. Healy, *Pharmaceutics*, 2020, **12**, 433, DOI: 10.3390/pharmaceutics12050433.

16 M. Pekdemir, I. N. Qader, Y. Aydogdu and M. Coşkun, *El-Cezerî Journal of Science and Engineering*, 2021, **8**, 1395–1404, DOI: 10.31202/ecjse.932313.

17 H. M. Alhusaiki-Alghamdi, *J. Mod. Phys.*, 2019, **10**, 487, DOI: 10.4236/jmp.2019.105034.

18 H. A. Jawad and A. Hashim, Nanosistemi, Nanomateriali, Nanotehnologii, 2022, **20**, 4.

19 F. L. Rashid, A. Hashim, A. Dulaimi, A. Hadi, H. Ibrahim, M. A. Al-Obaidi and A. Ameen, *J. Compos. Sci.*, 2024, **8**, 123, DOI: 10.3390/jcs8040123.

20 K. Sarada and K. Muraleedharan, *J. Therm. Anal. Calorim.*, 2016, **126**, 1809–1819, DOI: 10.1007/s10973-016-5709-y.

21 C. Xiao, L. Gao, M. Lu, H. Chen and L. Guo, *J. Dispersion Sci. Technol.*, 2011, **32**, 1145–1150, DOI: 10.1080/01932691.2010.498237.

22 J. Zhang, D. Jiang and Q. Lin, *J. Am. Ceram. Soc.*, 2005, **88**, 1054–1056, DOI: 10.1111/j.1551-2916.2005.00207.x.

23 C. Y. Chen and P. H. Hsiao, *ChemPhysChem*, 2015, **16**, 540–545, DOI: 10.1002/cphc.201402634.

24 C. S. Thompson and M. Zou, in *2013 IEEE 39th Photovoltaic Specialists Conference*, PVSC, 2013, pp. 1489–1491, DOI: 10.1109/PVSC.2013.6744427.

25 L. Gahramanli, M. Jafarov, M. Muradov, H. Shirinova, R. Khankishiyeva, S. Alakbarova, G. Eyvazova, M. B. Baghirov, N. Musayeva, V. Yevdokymenko and K. Dmytro, *J. Mater. Sci.*, 2025, 1–9, DOI: 10.1007/s10853-025-11503-3.

26 Q. Xu, R. Tu, Q. Sun, M. Yang, Q. Li, S. Zhang, L. Zhang, T. Goto, H. Ohmori, J. Shi and H. Li, *RSC Adv.*, 2019, **9**, 2426–2430, DOI: 10.1007/s10853-025-11503-3.

27 H. Liu, Z. Chai, K. Wei, S. de Moraes Shubeita, P. Wady, D. Shepherd, E. Jimenez-Melero and P. Xiao, *J. Eur. Ceram.*

28 B. Wang, X. Shang, J. Zhang, J. Shen, X. Wang and Z. Zhang, *Environ. Sci.:Adv.*, 2023, **2**, 132–139, DOI: 10.1039/D2VA00253A.

29 G. Luo, Z. Zhang, J. Hu, J. Zhang, Y. Sun, Q. Shen and L. Zhang, *Materials*, 2020, **13**, 1496, DOI: 10.3390/ma13071496.

30 H. M. Zidan, E. M. Abdelrazek, A. M. Abdelghany and A. E. Tarabiah, *J. Mater. Res. Technol.*, 2019, **8**, 904–913, DOI: 10.1016/j.jmrt.2018.04.023.

31 S. B. Gasha, M. Trautmann and G. Wagner, *Materials*, 2024, **17**, 435, DOI: 10.3390/ma17020435.

32 O. Folorunso, Y. Hamam, R. Sadiku and W. Kupolati, *J. Inorg. Organomet. Polym. Mater.*, 2024, **34**, 5667–5690, DOI: 10.1007/s10904-024-03179-0.

33 C. Gherasim, M. Asandulesa, N. Fifere, F. Doroftei, D. Tîmpu and A. Airinei, *Nanomaterials*, 2024, **14**, 759, DOI: 10.3390/nano14090759.

34 S. I. Kim, J. Y. Moon, S. Bae, Z. Xu, Y. Meng, J. W. Park, J. H. Lee and S. H. Bae, *Small Methods*, 2025, **9**, 2401551, DOI: 10.1002/smtd.202401551.

35 Y. Li, C. Chen, J. T. Li, Y. Yang and Z. M. Lin, *Nanoscale Res. Lett.*, 2011, **6**, 454, DOI: 10.1186/1556-276X-6-454.

36 G. Colston and M. Myronov, *Semicond. Sci. Technol.*, 2017, **32**, 114005, DOI: 10.1088/1361-6641/aa8b2a.

37 S. Kamath, G. H. Kumar, R. Chandramani and M. C. Radhakrishna, *Arch. Phys. Res.*, 2015, **6**, 18–21.

38 Y. Li, C. Chen, J. T. Li, Y. Yang and Z. M. Lin, *Nanoscale Res. Lett.*, 2011, **6**, 454, DOI: 10.1186/1556-276X-6-454.

39 S. Jiang, S. Gao, J. Kong, X. Jin, D. Wei, D. Li and P. Xing, *RSC Adv.*, 2019, **9**, 23785–23790, DOI: 10.1039/C9RA03383A.

40 R. P. D'Amelia, J. Mancuso and W. Nirode, *J. Polym. Biopolym. Phys. Chem.*, 2019, **7**, 1–9, DOI: 10.12691/jpbpc-7-1-1.

41 D. Lubasova, H. Niu, X. Zhao and T. Lin, *RSC Adv.*, 2015, **5**, 54481–54487, DOI: 10.1039/C5RA07514A.

42 I. A. Safo, M. Werheid, C. Dosche and M. J. Oezaslan, *Nanoscale Adv.*, 2019, **1**, 3095–3106, DOI: 10.1039/C9NA00186G.

43 A. M. Abdelghany, M. S. Meikhail, A. H. Oraby and M. A. Aboelwafa, *Polym. Bull.*, 2023, **80**, 13279–13298, DOI: 10.1007/s00289-023-04700-0.

44 A. Fuad, U. Kultsum and A. Taufiq, *Mater. Today: Proc.*, 2019, **17**, 1451–1457, DOI: 10.1016/j.matpr.2019.06.167.

45 A. Kleinová, J. Huran, V. Sasinková, M. Perný, V. Šály and J. Packa, in *Reliability of Photovoltaic Cells, Modules, Components, and Systems VIII*, SPIE, 2015, vol. 9563, pp. 166–173, DOI: 10.1117/12.2186748.

46 M. F. Omar, A. K. Ismail, I. Sumpono, E. A. Alim, M. N. Nawi, M. A. Mukri, Z. Othaman and S. Sakrani, Malaysian Journal of Fundamental and, *Appl. Sci.*, 2012, **8**, 4, DOI: 10.11113/mjfas.v8n4.156.

*Soc.*, 2024, **44**, 6305–6320, DOI: 10.1016/j.jeurceramsoc.2024.04.001.